

# *In vivo* anatomical imaging of colorectum by tens-of-micron-resolved photoacoustic/ultrasonic endoscope

Cite as: Appl. Phys. Lett. **118**, 153702 (2021); <https://doi.org/10.1063/5.0049855>

Submitted: 10 March 2021 . Accepted: 30 March 2021 . Published Online: 14 April 2021

Ting Guo,  Kedi Xiong, Zixin Zhang, Ling Li, and  Sihua Yang



View Online



Export Citation



CrossMark

## ARTICLES YOU MAY BE INTERESTED IN

[Substrate-controlled dynamics of spin qubits in low dimensional van der Waals materials](#)

Applied Physics Letters **118**, 154003 (2021); <https://doi.org/10.1063/5.0048399>

[Single-nanowire silicon photodetectors with core-shell radial Schottky junction for self-powering application](#)

Applied Physics Letters **118**, 153904 (2021); <https://doi.org/10.1063/5.0046096>

[Tunable band-pass optical vortex processor enabled by wash-out-refill chiral superstructures](#)

Applied Physics Letters **118**, 151102 (2021); <https://doi.org/10.1063/5.0041117>



Timing is everything.  
Now it's automatic.

A new synchronous source measure system for electrical measurements of materials and devices

 [Learn more](#)

# *In vivo* anatomical imaging of colorectum by tens-of-micron-resolved photoacoustic/ultrasonic endoscope

Cite as: Appl. Phys. Lett. **118**, 153702 (2021); doi: 10.1063/5.0049855

Submitted: 10 March 2021 · Accepted: 30 March 2021 ·

Published Online: 14 April 2021



View Online



Export Citation



CrossMark

Ting Guo,<sup>1,2</sup> Kedi Xiong,<sup>1,2,a)</sup>  Zixin Zhang,<sup>1,2</sup> Ling Li,<sup>1,2</sup> and Sihua Yang<sup>1,2</sup> 

## AFFILIATIONS

<sup>1</sup>MOE Key Laboratory of Laser Life Science and Institute of Laser Life Science, College of Biophotonics, South China Normal University, Guangzhou 510631, China

<sup>2</sup>Guangdong Provincial Key Laboratory of Laser Life Science, College of Biophotonics, South China Normal University, Guangzhou 510631, China

<sup>a)</sup>Author to whom correspondence should be addressed: [xiongkd2012@163.com](mailto:xiongkd2012@163.com)

## ABSTRACT

The existing photoacoustic/ultrasound (PA/US) endoscopes with compromise in lateral resolution were difficult to realize superior anatomical imaging. To obtain comprehensive biological information of the colorectum in a noninvasive manner, a tens-of-micron-resolved PA/US endoscope with a 360° field of view was developed. A coaxial structure, which ensures optical and acoustic foci aligned, was employed, and a PVDF-based focused transducer with a high frequency was applied. The endoscopic system achieved lateral resolutions of 16 μm (PA) and 73 μm (US), and axial resolution of 65 μm. Phantom and *ex vivo* experiments were performed to estimate the performance of the dual-modality endoscope. *In vivo* three-dimensional imaging of rabbit colorectum exhibited the intact vascular network at different depths from the mucosa of the colorectal wall to the mesentery, and the structures beneath them. Therefore, *in vivo* anatomical imaging demonstrates that the tens-of-micron-resolved PA/US endoscope holds great potential in the clinical detection of colorectal diseases.

Published under license by AIP Publishing. <https://doi.org/10.1063/5.0049855>

Colorectal diseases are multiple and similar in early symptoms, such as early bowel tumors and inflammation,<sup>1,2</sup> which made clinicians difficult to distinguish between intestinal diseases by using a single-modality endoscopy.<sup>3,4</sup> The occurrence of tumor and inflammation is commonly accompanied by abnormal proliferation and morphological changes of vessels, thickening, and edema of tissue.<sup>4</sup> In clinical application, endoscopic ultrasound (EUS) is the commonly used technique to diagnose intestinal diseases.<sup>5</sup> Although EUS could measure several millimeters and offered tissue information on organ lesions, it is limited in providing high-resolution information on vascular-related diseases.<sup>6</sup> Thus, an imaging modality with the capability of providing functional information is in urgent need to detect colorectal diseases.

Photoacoustic imaging (PAI) can provide functional<sup>7,8</sup> and molecular information<sup>9</sup> based on the endogenous optical chromophore of abundant biomolecules (such as lipid, hemoglobin, and DNA),<sup>10,11</sup> or nanoprobe,<sup>12–14</sup> with high spatial resolution at depths.<sup>15,16</sup> PA endoscopy (PAE),<sup>17,18</sup> as an important technical branch of PAI, succeeds in imaging organs with cavity by miniaturizing the imaging probe size,

which has the potential for providing complementary information to EUS, particularly for vessel imaging with decent resolution from superficial to deep tissue. Therefore, dual-modality endoscope that combined PA and US imaging is an efficient tool to distinguish the minor discrepancy between structure and morphology of tumor and other diseases.<sup>19</sup>

Without increasing the complexity of the PAE, a photoacoustic/ultrasonic (PA/US) dual-modality endoscope is developed through adding the ultrasound pulser/receiver modular, which could recognize the vascular network and tissue structure, and provide complementary information for each other. Yang *et al.* developed a series of PA/US endoscopes and obtained 3D *in vivo* images by micro-motor-based catheters.<sup>20–22</sup> Such technology progress is of great significance in terms of *in vivo* imaging research. However, the resolution close to one hundred results in blurry vascular network, and only part of the cross-sectional PA and US images could be obtained due to the blocking of the fronting wires. Although an optical-resolution PA endoscope is developed later, the endoscope only provides single-modality imaging.<sup>23</sup> Subsequently, Li *et al.* presented catheter-based PA/US endoscopes and achieved 3D images with a 360° field of view.

However, the microvascular morphology cannot be clearly visualized due to insufficient spatial resolution.<sup>24,25</sup> Although the catheter-based PA/US endoscope can access the electronic endoscope to detect the tissue, the miniature size and flexible structure result in the limited radial- and lateral-imaging field of view in large lumen, such as stomach and colorectum. Thus, for optimal detection strategy of micro vessels, it is proper to design the endoscope structure (rigid endoscope or flexible endoscope, and focused transducer or unfocused transducer) for high-resolution imaging according to applied organs. Although some rigid PA/US endoscopes were developed for large lumen imaging,<sup>26–29</sup> all the above dual-modality endoscopic imaging systems were unable to achieve high resolution both in PA and US imaging.

In this study, for colorectal imaging, we designed a rigid PA/US endoscope, which provides a large radial imaging range with a 360° field of view. By optimizing the structure of the probe and increasing the frequency of the transducer, the PA/US endoscope achieves a best lateral resolution of 16  $\mu\text{m}$  and 73  $\mu\text{m}$ , respectively, and axial resolution of 65  $\mu\text{m}$ . *In vivo* anatomical images exhibit high-resolution visualization of vasculature in the mucosa layer. And more, the structural information of colorectal layers (including mucosa, submucosa, muscularis, and serosa) can be distinguished by US images. In addition, the pattern of vascular networks from mesentery to mucosa and the

distribution of other surrounding structures were observed by this dual-modality endoscopic imaging with tens-of-micron resolution, which is highly promising for assisting precision diagnosis and treatment of intestinal lesions in clinical applications.

Figure 1 illustrates the overall setup of the dual-modality endoscope. The schematic diagram of the PA/US dual-modality system is shown in Fig. 1(a); the system employs a frequency-doubled Nd: YAG laser (Model DTL-319QT, Laser-export) for PA irradiation operating at 532 nm with a 10 ns pulse duration. The laser beam passed through a beam expanding and filtering and then focused into a single mode fiber (SMF) by a fiber-coupler (PAF-X-7-A, Thorlabs, USA). An FPGA is used to provide trigger signals to synchronize the laser and data acquisition system (DAS) at the maximum repetition rate of 10 kHz for PA imaging. Simultaneously, the trigger signals were delayed 10  $\mu\text{s}$  for US transmit/receiver (5073PR, Olympus) to conduct the US imaging. Both PA and US signals are amplified with a 50 dB low noise amplifier (LNA650, Rfbay, USA) sequentially, then digitized by a single channel data acquisition card at a 200 MHz sampling rate (M4i. 4420, Spectrum, Germany), and stored in the computer for imaging reconstruction finally. To acquire a high-resolution PA image, the cross-sectional images (B-scans) were reconstructed from 5000 A-lines signals. Furthermore, spiral three-dimensional images

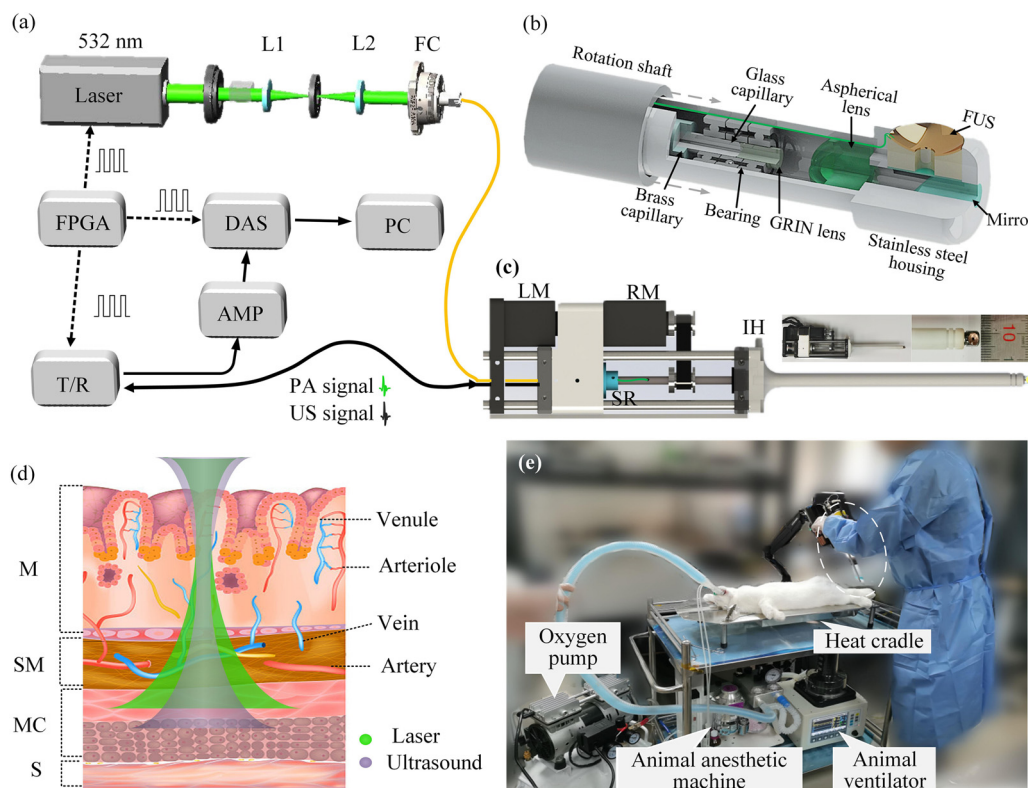


**FIG. 1.** System and structure of the dual-modality endoscope. (a) Schematic diagram of the dual-modality excitation and acquisition system. DAS, data acquisition system; L1 and L2, lens; FC, fiber coupler; AMP, amplifier; PC, personal computer; T/R, transmit and receive; FPGA, field programmable gate array. (b) Schematic structure of the endoscopic probe. FUS, focused ultrasonic transducer. (c) The schematic structure and photo of the PA/US dual-modality endoscope; LM, linear motor; RM, rotary motor; SR, slip ring; IH, injection hole. (d) Schematic diagram of optical excitation and PA signal generation by multi-layers structure of the colorectal wall. M, mucosa; SM, submucosa; MC, muscularis; S, serosa. (e) Photo of *in vivo* experiment equipment.

were obtained by a miniaturized linear motor. The fluency density of the output laser beam is controlled to  $16 \text{ mJ/cm}^2$ , which is 80% of the ANSI safety limit. All the operations mentioned above were controlled by the LabView® program on the computer. The three-dimensional (3D) front structure of the dual-modality probe with high-frequency focused transducer achieves the coaxial of laser and US focus, depicted in Fig. 1(b). The SMF passes through a brass capillary tube with a length of 20 cm and a glass capillary tube with a length of 1 cm in succession; the brass capillary covers the end of the glass capillary tube and is fixed with glue. The glass capillary is held by three multiple ball bearings, which provide a free rotation for the housing. A PVDF-based transducer with a central aperture of 1 mm and a size of 4.5 mm is designed. The transducer featured a  $9 \mu\text{m}$ -thickness PVDF element (Piezotech, France) to achieve acoustic focal length of 6.5 mm by compression molding. The output laser beam is weakly collimated by a GRIN lens, focused by an aspheric lens. A dielectric mirror at the optic axis reflects the laser beam to the target tissue [Fig. 1(d)] through the optical window of the transducer. A hard sheath is used to avoid the

rotating shaft contacting with tissue. The diameter of the hard sheath and the stainless-steel housing of the probe were designed to be 8 mm and 5.5 mm, respectively. Figure 1(c) shows the scanning structure of the dual-modality endoscope. In the process of imaging, the rotation and pullback of the probe are driven by a rotating motor and a stepper motor, respectively. A customized hollow electric slip ring (JINPAT, China) is used to transmit acoustic signals. The slip ring is designed with three paths: one for high-frequency signal transmission and two channels for shielding circuits. Figure 1(d) describes a structural diagram of colorectal wall and confocal mode with focused laser beam and acoustic beam, in which different tissue layers generate corresponding PA and US signals. The equipment presented in Fig. 1(e) includes oxygen pumps, animal ventilators, animal anesthetics, and hot cradles, which ensure the stability and health of the animals in *in vivo* experiments. All the animal experiments followed a protocol approved by the Institutional Review Board administered by the Human Research Protection Office at South China Normal University in Guangzhou.

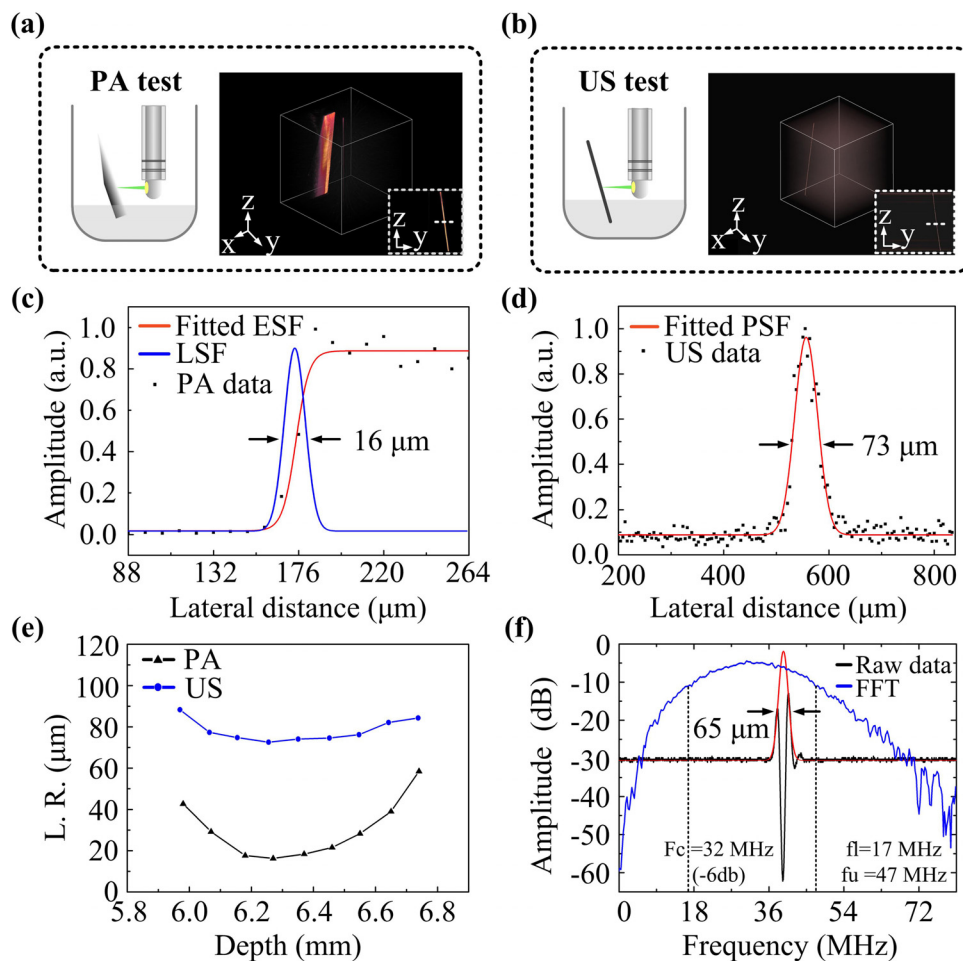


**FIG. 2.** Evaluation of the PA/US endoscopic system. (a) Experimental diagram and 3D PA image of the blade. (b) Experimental diagram and 3D US image of the tungsten wire. (c) PA lateral resolution of the endoscope. (d) US lateral resolution of the endoscope. (e) The lateral resolutions of the PA and US images at different depth. (f) Pulse response and the frequency spectrum of the transducer at the focus. FC, center frequency; fl, low frequency; fu, up frequency.

To validate the spatial resolution of the dual-modality endoscope, the experimental measurements were implemented. The sharp edge of a surgical blade and tungsten wire ( $10\ \mu\text{m}$ ) were imaged in PA and US imaging at different depths, respectively. Figures 2(a) and 2(b) show the schematic diagrams of the experiment and 3D images of the blade and tungsten wire, respectively, which were reconstructed from 500 B-scans using VolView® program. The sub-figures were maximum amplitude projection (MAP) images at z-y plane, whose white line is the focal position. As shown in Figs. 2(c) and 2(d), the best lateral resolution in PA and US image is  $\sim 16\ \mu\text{m}$  and  $\sim 73\ \mu\text{m}$  by calculating the full width at half-maximum (FWHM) of the line spread function (LSF) and point spread function (PSF), respectively. As is shown in Fig. 2(e), the lateral resolution of the PA (black) and US (blue) imaging obtained by the endoscope of the PVDF-based focused transducer at different imaging depths. The optical beam's depth of focus (DOF) is  $\sim 650\ \mu\text{m}$ , while the lateral resolution of US does not change significantly within this range. It is noted that the lateral resolution of US imaging is worse than the theoretical beam diameter of  $69\ \mu\text{m}$ , which is calculated by equation:<sup>30</sup>

$$\text{BD}(-6\text{dB}) = 1.02Fc/fD, \quad (1)$$

where  $F$  is the focal length,  $c$  is the material sound velocity,  $f$  is the frequency, and  $D$  is the element diameter. Figure 2(f) shows the pulse echoes signal and the frequency spectrum of focused transducer. The transducer provides bandwidth from about 17–47 MHz (93.7%

fractional bandwidth) at  $-6\ \text{dB}$ , whose center frequency is  $\sim 32\ \text{MHz}$ . Benefit from the wideband frequency response (blue) of PVDF-based transducer, the axial resolution is estimated to be  $63\ \mu\text{m}$  through calculating the FWHM of a typical Hilbert-transformed time-resolved US signal [Fig. 2(f)].

The imaging performance of the endoscope was evaluated by an imaging experiment of the simulated vein and *ex vivo* colorectum; the superior dual-modality spatial resolution and quality of image achieved by the endoscope are visible in the images (Fig. 3). The leaf was fixed in agar with the shape of a regular round tube. The endoscope conducted the pullback with a step size of  $6\ \mu\text{m}$ , and the scanning time is  $\sim 10\ \text{min}$ . Figures 3(a) and 3(b) present the PA RMAP and US RMAP images of the leaf, respectively. In PA and US images, the veins of leaf are one-to-one correspondence. The fused PA and US cross-sectional (B-scan) image of the colorectum in polar coordinate is shown in Fig. 3(c) to reveal the layered architecture. It can be seen that based on the high axial resolution of the US image, various layers could be clearly distinguished, which is consistent with the histological image in Fig. 3(e). The fused image in Fig. 3(d) could only observe part of the large blood vessels mainly in submucosa due to the loss of blood in *ex vivo* sample. In the locally enlarged fused image shown in Fig. 3(d), it is obvious to identify the mucosa, submucosa, muscularis, and the boundary between the sample and the agar used for immobilization. Notably, the boundary between the circular muscle and longitudinal muscle in the muscularis, marked by the orange arrow, was

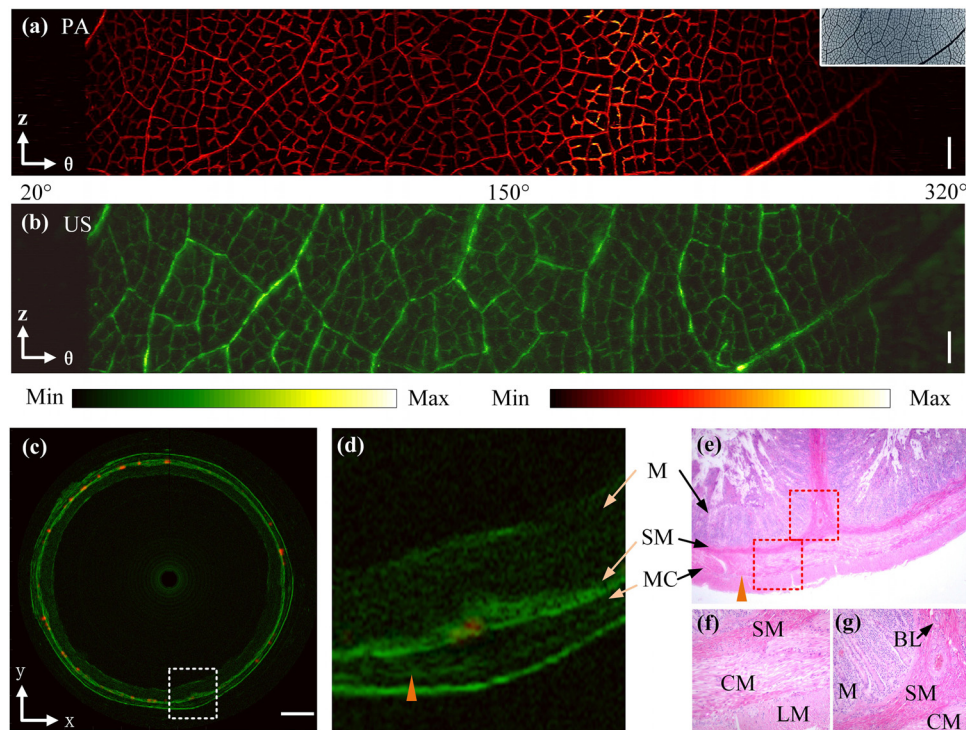


**FIG. 3.** *Ex vivo* experiments for evaluating imaging resolution. (a) PA-RMAP of leaf phantom angular transformed to a Cartesian coordinate system in 300 degrees. Scale bar, 1.5 mm. (b) US-RMAP of leaf phantom angular transformed to a Cartesian coordinate system in 300°. Scale bar, 1.5 mm. (c) PA and US fused B-scan image. Scale bar, 2 mm. (d) Magnified images of the marked zones in (c). M, mucosa; SM, submucosa; MC, muscularis; CM, circular muscle; LM, longitudinal muscle. (e) Histologic images (H&E stain) of the colorectum. (f) and (g) Magnified images of the marked zones in (e).

even observed in the fused B-scan image relied on the high resolution. Figures 3(f) and 3(g) show magnified histological images of the marked area in red-dotted line in Fig. 3(e).

To further demonstrate the *in vivo* imaging capacity of the tens-of-micron-resolved dual-modality endoscope, a New Zealand White rabbit was performed for *in vivo* experiment. The rabbit fasted 24 h before the experiment to reduce the residual excreta. The anesthesia respirator was used to actively control breathing frequency and strength of animals during the *in vivo* imaging process. Figure 4(a) shows a fused B-scan image of the rabbit's colorectum, which clearly presents distribution of blood vessels in the colorectal wall. Figures 4(b) and 4(c) show the photoacoustic and ultrasound B-scan, in which the PA image is encoded by true-depth. The enlarged images in Figs. 4(b) and 4(c) were presented in Figs. 4(d) and 4(e), respectively. It can be seen that the blood vessels enlarged as the depth increases and could be distinguished from those in other parenteral tissues according to the structure information provided by the corresponding ultrasound images in Fig. 4(f). It is obvious that two hyperechoic areas at the shallowest layer are the boundary between the balloon and colorectal wall. The submucosa of the colorectum presents hyperechoic areas, while the mucosa and muscularis present hypoechoic areas (white arrow).

To better depict detailed information on *in vivo* anatomical images, photoacoustic and ultrasound data were encoded, 3D rendered, and projected, as shown in Fig. 5. The 3D scanning imaging was conducted with a step size of 10  $\mu\text{m}$  and scanning time of 448 s. Different from the depth encoded in photoacoustic microscopy, the true-depth encoded of vasculature based on the colorectal surface was shown in Fig. 5(a); the dense vascular network and different sizes demonstrate that blood vessels distributed in different-layered architecture. Figure 5(b) shows the 3D rendering of blood vessel. Although the large fluctuation of colorectal surface, 3D rendering image clearly exhibits

the trend of the blood vessels, which spread into the colorectal wall from the mesentery and form the left and right blood vessels branches. Magnified image of the marked area in Fig. 5(b) is shown in Fig. 5(c), which exhibits the rich capillaries, micro-vessels, and arteriovenous vessels from superficial to deep. As shown in the 3D-rendered US image [Fig. 5(d)], the architecture in colorectal wall could be clearly observed, besides the adjacent organs and bones outside the rectum in the abdominal cavity are also displayed, such as ovaries, pubes, and tailbone (white arrows).<sup>31</sup> Figure 5(e) presents the top view of Fig. 5(d), the ventral view of ovaries, and pubes, and the structure of obturator foramen could obviously be revealed.<sup>32</sup> In order to observe the complete organ structure, the US image in Fig. 5(e) redefines the initial position of the polar coordinates, equivalent to translate image in angular direction. Thus, the high spatial resolution enables the PA/US dual-modality endoscope to intuitively and accurately visualize the vascular system and colorectal structure in *in vivo* imaging method.

In summary, we demonstrate the high-resolution *in vivo* anatomical imaging including structural and vascular network information for colorectum by a tens-of-micron-resolved dual-modality PA/US endoscope, which has a large radial imaging range with a 360° field of view. The system has achieved the most abundant vascular system of colorectum in photoacoustic endoscopy. And the morphology of blood vessels from mesentery to mucosa and the distribution of other tissues in its neighborhood were observed by the PA/US dual-modality endoscope. Actually, the anesthesia respirator was used to actively control the breathing frequency and strength of animals during the *in vivo* imaging process, but the breathing, heart, and intestinal peristalsis are random and inevitable.<sup>33</sup> Some work will be conducted to achieve more superior imaging of the vascular network and physiological structure of colorectum. First, the imaging speed needs to be further improved by increasing the repetition rate of laser. Second, improving the image reconstruction algorithm to eliminate the

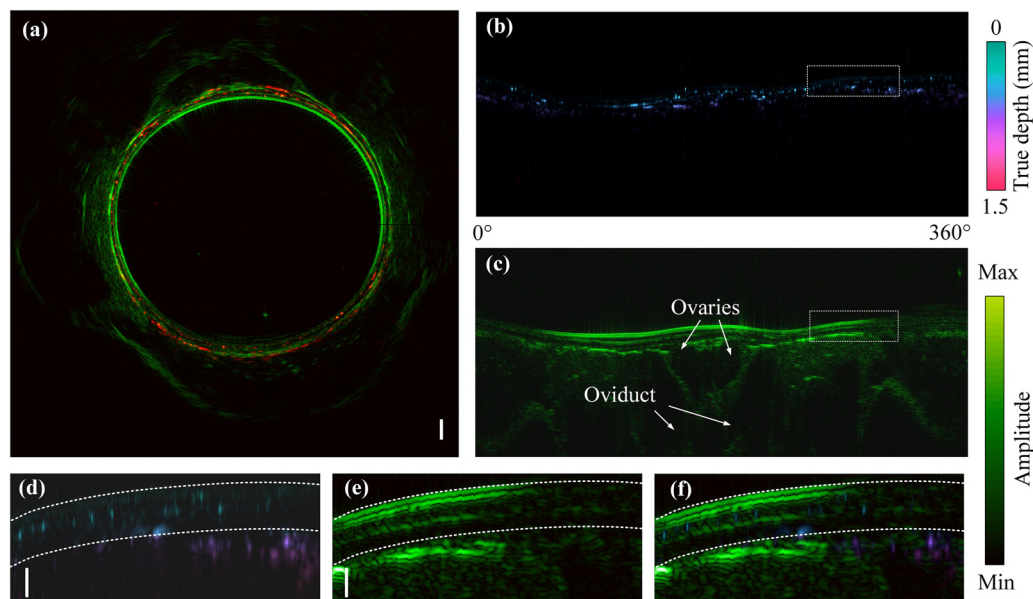


**FIG. 4.** PA/US B-scan images acquired from *in vivo* rabbit colorectum. (a) Fused B-scan image in a polar coordinate system. Scale bar, 1 mm. (b) and (c) PA and US B-scan images in a Cartesian coordinate system. (d) and (e) Partial enlarged image marked zones in (b) and (c). Scale bar, 300  $\mu\text{m}$ . (f) Fused image of (d) and (e).

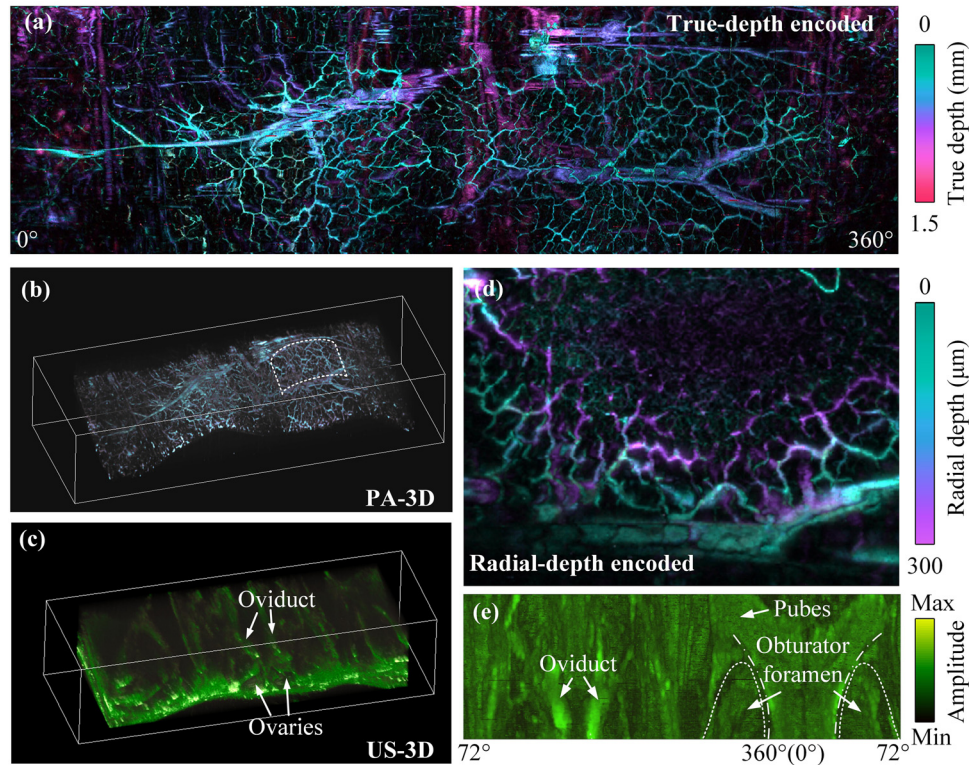


**FIG. 5.** 3D *in vivo* imaging of rabbit colorectum. (a) True-depth encoded image. (b) 3D rendering image of colorectum. (c) Magnified image of the marked area in (b). (d) 3D US images of the colorectum in Cartesian coordinate system. (e) Top view from (d).

dislocation caused by dithering dislocation;<sup>34–36</sup> these approaches will greatly improve the image quality. In addition, this study has proved that the *in vivo* anatomical imaging indicates a good application prospect for assisting precision diagnosis and the treatment of colorectal disease. Related research will be carried out later.

See the [supplementary material](#) for the 3D vascular network and local vascular tomography.

This research is supported by the National Natural Science Foundation of China (Nos. 62005084, 61822505, 11774101, and 61627827), the Science and Technology Planning Project of Guangdong Province, China (No. 2015B020233016), China Postdoctoral Science Foundation (No. 2019M652943), the Natural Science Foundation of Guangdong Province, China (No. 2019A1515011399), and the Science and Technology Program of Guangzhou (No. 2019050001).

#### DATA AVAILABILITY

The data that support the findings of this study are available from the corresponding author upon reasonable request.

#### REFERENCES

- M. J. Waldner, F. Knieling, C. Egger, S. Morscher, J. Claussen, and M. Vetter, "Multispectral optoacoustic tomography in crohn's disease: Noninvasive imaging of disease activity," *Gastroenterology* **151**, 238 (2016).
- E. Kuipers, W. Grady, D. Lieberman, D. Lieberman, T. Seufferlein, J. J. Sung, P. G. Boelens, C. J. H. van de Velde, and T. Watanabe, "Colorectal cancer," *Nat. Rev. Dis. Primers* **1**, 15065 (2015).
- Y. Li, Z. Zhu, J. J. Chen, J. C. Jing, C.-H. Sun, S. Kim, and Z. Chen, "Multimodal endoscopy for colorectal cancer detection by optical coherence tomography and near-infrared fluorescence imaging," *Biomed. Opt. Express* **10**, 2419 (2019).
- M. Omar, J. Aguirre, and V. Ntziachristos, "Optoacoustic mesoscopy for biomedicine," *Nat. Biomed. Eng.* **3**, 354 (2019).
- X. Wang, V. Seetohul, R. Chen, Z. Zhang, M. Qian, Z. Shi, G. Yang, P. Mu, C. Wang, Z. Huang, Q. Zhou, H. Zheng, S. Cochran, and W. Qiu, "Development of a mechanical scanning device with high-frequency ultrasound transducer for ultrasonic capsule endoscopy," *IEEE Trans. Med. Imaging* **36**, 1922 (2017).
- T. Thomas, D. Gilbert, P. V. Kaye, I. Penman, G. P. Aithal, and K. Ragnath, "High-resolution endoscopy and endoscopic ultrasound for evaluation of early neoplasia in Barrett's esophagus," *Surg. Endosc.* **24**, 1110 (2010).
- J. B. Chen, Y. C. Zhang, L. Y. He, Y. Z. Liang, and L. D. Wang, "Wide-field polygon-scanning photoacoustic microscopy of oxygen saturation at 1-MHz A-line rate," *Photoacoustics* **20**, 100195 (2020).
- J. Shepherd, G. Renaud, P. Clouzet, and K. van Wijk, "Photoacoustic imaging through a cortical bone replica with anisotropic elasticity," *Appl. Phys. Lett.* **116**, 243704 (2020).
- R. H. Chen, S. S. Huang, T. T. Lin, H. S. Ma, W. J. Shan, F. Duan, J. Lv, J. D. Zhang, L. Ren, and L. M. Nie, "Photoacoustic molecular imaging-escorted adipose photodynamic-browning synergy for fighting obesity with virus-like complexes," *Nat. Nanotechnol.* (published online 2021).
- Z. Piao, T. Ma, J. Li, M. T. Wiedmann, S. Huang, M. Yu, K. K. Shung, Q. Zhou, C. Kim, and Z. Chen, "High speed intravascular photoacoustic imaging with fast optical parametric oscillator laser at 1.7  $\mu\text{m}$ ," *Appl. Phys. Lett.* **107**, 083701 (2015).

- <sup>11</sup>S. Mezil, A. M. Caravaca-Aguirre, E. Z. Zhang, P. Moreau, I. Wang, P. C. Beard, and E. Bossy, "Single-shot hybrid photoacoustic-fluorescent microendoscopy through a multimode fiber with wavefront shaping Biomed," *Biomed. Opt. Express* **11**, 5717 (2020).
- <sup>12</sup>Y. Chen, Y. Zhao, and S. J. Yoon, "Miniature gold nanorods for photoacoustic molecular imaging in the second near-infrared optical window," *Nat. Nanotechnol.* **14**, 465 (2019).
- <sup>13</sup>H. Zhang, S. Huang, and Y. Chen, "Examining the technical feasibility of prostate cancer molecular imaging by transrectal photoacoustic tomography with transurethral illumination," *Exp. Biol. Med.* **245**, 313 (2020).
- <sup>14</sup>C. Xie, X. Zhen, Y. Lyu, and K. Pu, "Nanoparticle regrowth enhances photoacoustic signals of semiconducting macromolecular probe for *in vivo* imaging," *Adv. Mater.* **29**, 1703693.1 (2017).
- <sup>15</sup>H. Kim, J. W. Baik, S. W. Jeon, J. Y. Kim, and C. H. Kim, "PAExM: Label-free hyper-resolution photoacoustic expansion microscopy," *Opt. Lett.* **45**, 6755 (2020).
- <sup>16</sup>W. T. Zhou, Y. C. Hu, Z. J. Chen, and D. Xing, "All-optical photoacoustic and reflectance confocal microscopy for melanoma characterization," *Appl. Phys. Lett.* **114**, 163704 (2019).
- <sup>17</sup>X. W. Li, K. D. Xiong, and S. H. Yang, "Large-depth-of-field optical-resolution colorectal photoacoustic endoscope," *Appl. Phys. Lett.* **114**, 163703 (2019).
- <sup>18</sup>H. Guo, G. Song, H. Xie, and L. Xi, "Photoacoustic endomicroscopy based on a MEMS scanning mirror," *Opt. Lett.* **42**, 4615 (2017).
- <sup>19</sup>M. Yang, L. Zhao, F. Yang, M. Wang, N. Su, C. Zhao, Y. Gui, Y. Wei, R. Zhang, J. Li, T. Han, X. He, L. Zhu, H. Wu, C. Li, and Y. Jiang, "Quantitative analysis of breast tumours aided by three-dimensional photoacoustic/ultrasound functional imaging," *Sci. Rep.* **10**, 8047 (2020).
- <sup>20</sup>J. M. Yang, R. Chen, C. Favazza, J. Yao, C. Li, Z. Hu, Q. Zhou, K. K. Shung, and L. V. Wang, "A 2.5-mm diameter probe for photoacoustic and ultrasonic endoscopy," *Opt. Express* **20**, 23944 (2012).
- <sup>21</sup>J. M. Yang, C. Favazza, J. Yao, R. Chen, Q. Zhou, K. K. Shung, and L. V. Wang, "Three-dimensional photoacoustic endoscopic imaging of the rabbit esophagus," *PLoS One* **10**, e0120269 (2015).
- <sup>22</sup>J. M. Yang, C. Favazza, R. Chen, J. Yao, X. Cai, K. Maslov, Q. Zhou, K. K. Shung, and L. V. Wang, "Simultaneous functional photoacoustic and ultrasonic endoscopy of internal organs *in vivo*," *Nat. Med.* **18**, 1297 (2012).
- <sup>23</sup>J. M. Yang, C. Li, R. Chen, B. Rao, J. Yao, C. Yeh, A. Danielli, K. Maslov, Q. Zhou, K. K. Shung, and L. V. Wang, "Optical-resolution photoacoustic endomicroscopy *in vivo*," *Biomed. Opt. Express* **6**, 918 (2015).
- <sup>24</sup>Y. Li, R. Q. Lin, C. B. Liu, J. H. Chen, H. D. Liu, R. Q. Zheng, X. J. Gong, and L. Song, "*In vivo* photoacoustic/ultrasonic dual-modality endoscopy with a miniaturized full field of-view catheter," *J. Biophotonics* **11**, e201870164 (2018).
- <sup>25</sup>Y. Li, Z. Zhu, J. C. Jing, J. J. Chen, A. E. Heidari, Y. He, J. Zhu, T. Ma, M. Yu, Q. Zhou, and Z. Chen, "High-speed integrated endoscopic photoacoustic and ultrasound imaging system," *IEEE J. Sel. Top. Quantum Electron.* **25**, 1 (2019).
- <sup>26</sup>M. Basij, A. Karpiouk, I. Winer, S. Emelianov, and M. Mehrmohammadi, "Dual-illumination ultrasound/photoacoustic endoscopic system," in IEEE International Ultrasonics Symposium (2020), Vol. 13, p. 6900310.
- <sup>27</sup>H. Lei, L. A. Johnson, K. A. Eaton, S. C. Liu, J. Ni, X. D. Wang, P. D. R. Higgins, and G. Xu, "Characterizing intestinal strictures of Crohn's disease *in vivo* by endoscopic photoacoustic imaging," *Biomed. Opt. Express* **10**, 2542 (2019).
- <sup>28</sup>B. Cong, C. Qiu, Y. Ren, Y. Bai, M. Xing, T. Yin, X. Gong, L. Song, R. Zheng, and C. Liu, "A low cost sensitive transrectal photoacoustic probe with single-fiber bright-field illumination for *in vivo* canine prostate imaging and real-time biopsy needle guidance," *IEEE Sens. J.* **20**, 10974 (2020).
- <sup>29</sup>X. Dai, H. Yang, T. Shan, H. K. Xie, S. A. Berceli, and H. Jiang, "Miniature endoscope for multimodal imaging," *ACS Photonics* **4**, 174 (2017).
- <sup>30</sup>N. Olympus, *Ultrasonic Transducers Technical Notes* (Olympus NDT, 2006).
- <sup>31</sup>F. Stan, A. Damian, A. Gudea, C. Dezdrobotu, D. Bob, C. Martonos, I. Bochis, and B. Pogana, "Comparative anatomical study of the large intestine in rabbit and chinchilla," *Bull. Univ. Agric. Sci. Vet. Med. Cluj-Napoca, Vet. Med.* **71**, 208 (2014).
- <sup>32</sup>Ö. Özgel, E. Karakurum, Y. Demiraslan, and M. Aykut, "The effect of stomach's different fullness levels on the topography of intestines in New Zealand rabbit," *Eurasian J. Vet. Sci.* **33**, 8 (2017).
- <sup>33</sup>J. Mavadia-Shukla, P. Fathi, W. Liang, S. Wu, C. Sears, and X. Li, "High-speed, ultrahigh-resolution distal scanning OCT endoscopy at 800 nm for *in vivo* imaging of colon tumorigenesis on murine models," *Biomed. Opt. Express* **9**, 3731 (2018).
- <sup>34</sup>B. Wang, N. Wei, K. Peng, and J. Xiao, "Modified back-projection method in acoustic resolution-based photoacoustic endoscopy for improved lateral resolution," *Med. Phys.* **45**, 4430 (2018).
- <sup>35</sup>N. Davoudi, X. L. Deán-Ben, and D. Razansky, "Deep learning photoacoustic tomography with sparse data," *Nat. Mach. Intell.* **1**, 453 (2019).
- <sup>36</sup>H. G. Lan, D. H. Jiang, C. C. Yang, F. Gao, and F. Gao, "Y-Net: Hybrid deep learning image reconstruction for photoacoustic tomography *in vivo*," *Photoacoustics* **20**, 100197 (2020).